Neurobiology of Disease 111 (2018) 59–69

Contents lists available at ScienceDirect

Neurobiology of Disease

journal homepage: www.elsevier.com/locate/ynbdi

Inhibition of histone deacetylase 6 (HDAC6) protects against vincristine-induced peripheral neuropathies and inhibits tumor growth

Lawrence Van Helleputte[a,b], Mandy Kater[a,b], Dana P. Cook[c], Caroline Eykens[a,b], Elisabeth Rossaert[a,b], Wanda Haeck[a,b], Tom Jaspers[a,b], Natasja Geens[a,b], Pieter Vanden Berghe[d], Conny Gysemans[c], Chantal Mathieu[c], Wim Robberecht[a,b,e], Philip Van Damme[a,b,e], Guido Cavaletti[f], Matthew Jarpe[g], Ludo Van Den Bosch[a,b,*]

[a] KU Leuven - University of Leuven, Department of Neurosciences, Experimental Neurology, Leuven Research Institute for Neuroscience and Disease (LIND), Leuven, Belgium
[b] VIB, Center for Brain & Disease Research, Laboratory of Neurobiology, Leuven, Belgium
[c] KU Leuven - University of Leuven, Clinical and Experimental Endocrinology, Leuven, Belgium
[d] KU Leuven - University of Leuven, Laboratory for Enteric Neuroscience, TARGID, Leuven, Belgium
[e] University Hospitals Leuven, Department of Neurology, Leuven, Belgium
[f] Experimental Neurology Unit and Milan Center for Neuroscience, School of Medicine and Surgery, University of Milano-Bicocca, Monza, Italy
[g] Acetylon Pharmaceuticals Inc., Boston, MA, USA

ARTICLE INFO

Keywords:
Cancer
Chemotherapy
Axonal transport
Pain
Acetylation
Microtubules

ABSTRACT

As cancer is becoming more and more a chronic disease, a large proportion of patients is confronted with devastating side effects of certain anti-cancer drugs. The most common neurological complications are painful peripheral neuropathies. Chemotherapeutics that interfere with microtubules, including plant-derived vinca-alkaloids such as vincristine, can cause these chemotherapy-induced peripheral neuropathies (CIPN). Available treatments focus on symptom alleviation and pain reduction rather than prevention of the neuropathy. The aim of this study was to investigate the potential of specific histone deacetylase 6 (HDAC6) inhibitors as a preventive therapy for CIPN using multiple rodent models for vincristine-induced peripheral neuropathies (VIPN). HDAC6 inhibition increased the levels of acetylated α-tubulin in tissues of rodents undergoing vincristine-based chemotherapy, which correlates to a reduced severity of the neurological symptoms, both at the electrophysiological and the behavioral level. Mechanistically, disturbances in axonal transport of mitochondria is considered as an important contributing factor in the pathophysiology of VIPN. As vincristine interferes with the polymerization of microtubules, we investigated whether disturbances in axonal transport could contribute to VIPN. We observed that increasing α-tubulin acetylation through HDAC6 inhibition restores vincristine-induced defects of axonal transport in cultured dorsal root ganglion neurons. Finally, we assured that HDAC6-inhibition offers neuroprotection without interfering with the anti-cancer efficacy of vincristine using a mouse model for acute lymphoblastic leukemia. Taken together, our results emphasize the therapeutic potential of HDAC6 inhibitors with beneficial effects both on vincristine-induced neurotoxicity, as well as on tumor proliferation.

1. Introduction

Chemotherapy-induced peripheral neuropathies are the most common neurological side effects of anti-cancer treatments with an incidence of up to 80% (Cavaletti et al., 2011; Seretny et al., 2014). Chemotherapeutics that interfere with microtubules, including the plant-derived taxanes and vinca-alkaloids, cause these peripheral neuropathies (Jaggi and Singh, 2012; Kannarkat et al., 2007). Vincristine is such a chemotherapeutic drug that belongs to the family of vinca-alkaloids and despite being the most neurotoxic drug of its class, vincristine is remarkably effective and therefore still widely used to treat hematological cancers (Gennery, 1985). Vincristine-induced neurotoxicity primarily affects large sensory nerves leading to dysesthesia and paresthesia, reduced electrophysiological response of the sural nerve and decreased intra-epidermal nerve fiber densities (Grisold et al., 2012). In more severe forms, motor problems also arise (Baron, 2006; Park et al., 2013). Symptoms of vincristine-induced peripheral neuropathies (VIPN) are dose dependent, arise progressively in a

* Corresponding author at: Laboratory of Neurobiology, Campus Gasthuisberg O&N4, PB602, Herestraat 49, B-3000 Leuven, Belgium.
E-mail address: ludo.vandenbosch@kuleuven.vib.be (L. Van Den Bosch).

https://doi.org/10.1016/j.nbd.2017.11.011
Received 13 July 2017; Received in revised form 13 October 2017; Accepted 27 November 2017
Available online 29 November 2017

stocking-glove type distribution and persist even after the treatment has been ceased (= coasting) (Schneider et al., 2015). Due to the enormous impact on the quality of life, the threshold for clinical toxicity depends on VIPN and could require excessive pain treatment or early cessation of the anti-cancer therapy (Gennery, 1985). To date, little is known about the pathophysiology of VIPN and no effective cure is available. Instead, management is limited to pain relief with anti-epileptics, anti-depressants and opioids, which can induce a myriad of side effects (Zareba, 2009). Therefore, a high medical need for an effective treatment for chemotherapy-induced peripheral neuropathies still exists (Cavaletti and Marmiroli, 2010; Majithia et al., 2016).

Vincristine exerts its anti-cancer effect by inhibiting the assembly of microtubules. These highly dynamic structures, composed of α- and β-tubulin heterodimers, play an important role in multiple cellular processes, including cytoskeleton homeostasis, mitosis, cell migration and intracellular trafficking (Lawson and Carazo Salas, 2013). Microtubule dynamics is also of pivotal importance in post-mitotic neurons (Conde et al., 2009; Stanton et al., 2011). These polarized cells rely on intact microtubules for neuronal architecture, but they also function as tracks for axonal transport between the cell body and synapses. Moreover, disturbances in axonal transport are a common hallmark in a variety of neurodegenerative disorders and peripheral neuropathies (Cashman and Höke, 2015; d'Ydewalle et al., 2011; De Vos and Hafezparast, 2017; Holzbaur and Scherer, 2011; Prior et al., 2017). As vincristine alters microtubule dynamics, axonal transport in neurons might also be affected and could contribute to the neurotoxicity observed in patients.

One of the key mechanisms regulating axonal transport in neurons are post-translational modifications of α- and β-tubulin. Especially acetylation at the ε-amino group of lys-40 of α-tubulin influences axonal transport (Dompierre et al., 2007). Increased levels of acetylation functions as a recruitment cue and improves the docking of motor proteins to microtubules (Reed et al., 2006). As such, α-tubulin acetylation is tightly regulated by α-tubulin acetyltransferases (αTATs) and histone deacetylase 6 (HDAC6), a member of the class IIb histone deacetylases. Unlike conventional histone deacetylases, HDAC6 is mostly localized in the cytoplasm, has a duplication of its catalytic deacetylase domain and a poly-ubiquitin associated zinc finger domain (Grozinger et al., 1999). These unique features allow HDAC6 to interact with substrates other than histones, including α-tubulin (Hubbert et al., 2002; Zhang et al., 2003). Although there is a correlation between microtubule dynamics and acetylation of α-tubulin (Almeida-Souza et al., 2011), it is still unclear how one impacts the other and how HDAC6 is involved in this process.

We previously observed that inhibition of the deacetylating function of HDAC6 rescues the phenotype of several mouse models for inherited peripheral neuropathies (Benoy et al., 2016, 2015; d'Ydewalle et al., 2011). HDAC6 inhibition effectively restored deficits in axonal transport in dorsal root ganglion (DRG) neurons isolated from Charcot-Marie-Tooth disease (CMT) type 2 mouse models (Benoy et al., 2016, 2015; d'Ydewalle et al., 2011; Shen et al., 2016). Due to the phenotypic resemblance of patients diagnosed with CMT and those with VIPN, we hypothesized that vincristine could induce axonal problems by interfering with microtubule dynamics. Interestingly, mitochondrial dysfunction also contributes to cisplatin-induced peripheral neuropathy, a different form of CIPN. Cisplatin treatment results in the depletion of the mitochondrial GTPase mitofusin-2 (MFN2), a protein associated with CMT2A (Bobylev et al., 2017; Züchner et al., 2004). The importance of mitochondrial dysfunction in peripheral neuropathy was further emphasized by the fact that cisplatin not only binds nuclear but also mitochondrial DNA (mtDNA), resulting in mitotoxicity in neurons (Podratz et al., 2017). In a recent study, mitochondrial bioenergetics, their axonal transport and the cisplatin-induced phenotype was completely restored using ACY-1083, another HDAC6-specific inhibitor (Krukowski et al., 2017). Therefore, the aim of this study was to investigate whether inhibition of HDAC6 could increase the acetylation of α-tubulin, rescue axonal transport deficits and prevent the development of VIPN.

The use of HDAC6 inhibitors is also a hot topic in cancer research. Specific HDAC6 inhibitors have been developed for the treatment of multiple myeloma and are currently tested in clinical trials (Santo et al., 2012). Generally, most research focuses on neuroprotection regardless of cancer, or on the anti-cancer efficacy, neglecting the neurotoxicity. As HDAC6 has been implicated in neurodegeneration as well as in cancer, we investigated both the neuroprotective effects and assured the anti-cancer efficacy of vincristine in combination with HDAC6 inhibitors. We found that HDAC6 inhibition has beneficial effects on both aspects.

2. Results

2.1. Pharmacological inhibition of HDAC6 protects against VIPN

Using a mouse model for VIPN, we observed that weekly administration of vincristine (500 μg/kg, ip) resulted in a progressive sensory peripheral neuropathy, characterized by decreased sensory nerve action potential (SNAP) amplitudes of the caudal nerve that stabilized after 4 weeks of treatment (Supplemental Fig. S1A). Nerve conduction velocities were unaffected, suggesting vincristine primarily affects the axons of peripheral nerves (Supplemental Fig. S1B). On the behavioral level, we used the Electronic Von Frey (EVF) test to determine the response to mechanical stimuli. The electrophysiological changes correlated with a hypersensitivity when applying pressure to the hind paw of mice treated with vincristine (Supplemental Fig. S1C). Vincristine toxicity was limited to the sensory nervous system as innervation of the neuromuscular junctions at the gastrocnemius muscle was normal and as no changes in rotarod performance, CMAP amplitudes or latencies were observed during the treatment (Supplemental Fig. S1, D–H).

Next, we investigated whether HDAC6 inhibition had an effect on the pathophysiology of VIPN using a small molecule, ACY-738, that specifically inhibits the deacetylating function of HDAC6 (Jochems et al., 2014). The severity of the sensory axonopathy was significantly reduced in mice that were co-treated with vincristine and ACY-738. Both the decrease in SNAP amplitudes and the mechanical hypersensitivity were significantly, although partially, restored (Fig. 1, A and B). We validated these findings using a second HDAC6-specific inhibitor, Tubastatin A (Butler et al., 2010), emphasizing the specific contribution of HDAC6 to the assessment of VIPN (Fig. 1, A and B). Also in a rat model for VIPN, we confirmed that inhibition of HDAC6 significantly reduced the symptoms induced by vincristine, both at the electrophysiological and at the behavioral level with 23.5% and 43.1% respectively (Supplemental Fig. S2).

As VIPN is considered a “dying-back” neuropathy (Silva et al., 2006), we evaluated the effect of HDAC6 inhibition on vincristine-induced defects at the most distal part of the peripheral nervous system. Analyzing skin biopsies of mice treated with vincristine alone or in combination with a HDAC6 inhibitor for the presence of the pan-neuronal marker, protein gene product 9.5 (PGP9.5), shows that HDAC6 inhibition restored PGP9.5 expression in the glabrous skin of the hind paw (Fig. 1, C and D). Histological examination confirmed that HDAC6-inhibition completely preserved the intra-epidermal nerve fiber density in animals treated with vincristine (Fig. 1, E–I and Supplemental Movies S1–S4). All together, these results show that HDAC6 inhibitors can reduce the severity of vincristine-induced neurotoxicity *in vivo*.

2.2. HDAC6 inhibition increases acetylated α-tubulin in vivo

Next, we determined the level of acetylated α-tubulin, the major substrate for HDAC6 (Hubbert et al., 2002; Zhang et al., 2003), in tissues isolated from mice that underwent chemotherapy with vincristine alone or in combination with ACY-738. Vincristine slightly reduced α-tubulin acetylation exclusively in sensory tissues (saphenous nerve and DRGs), but not in the sciatic nerve or spinal cord (Fig. 2). These findings

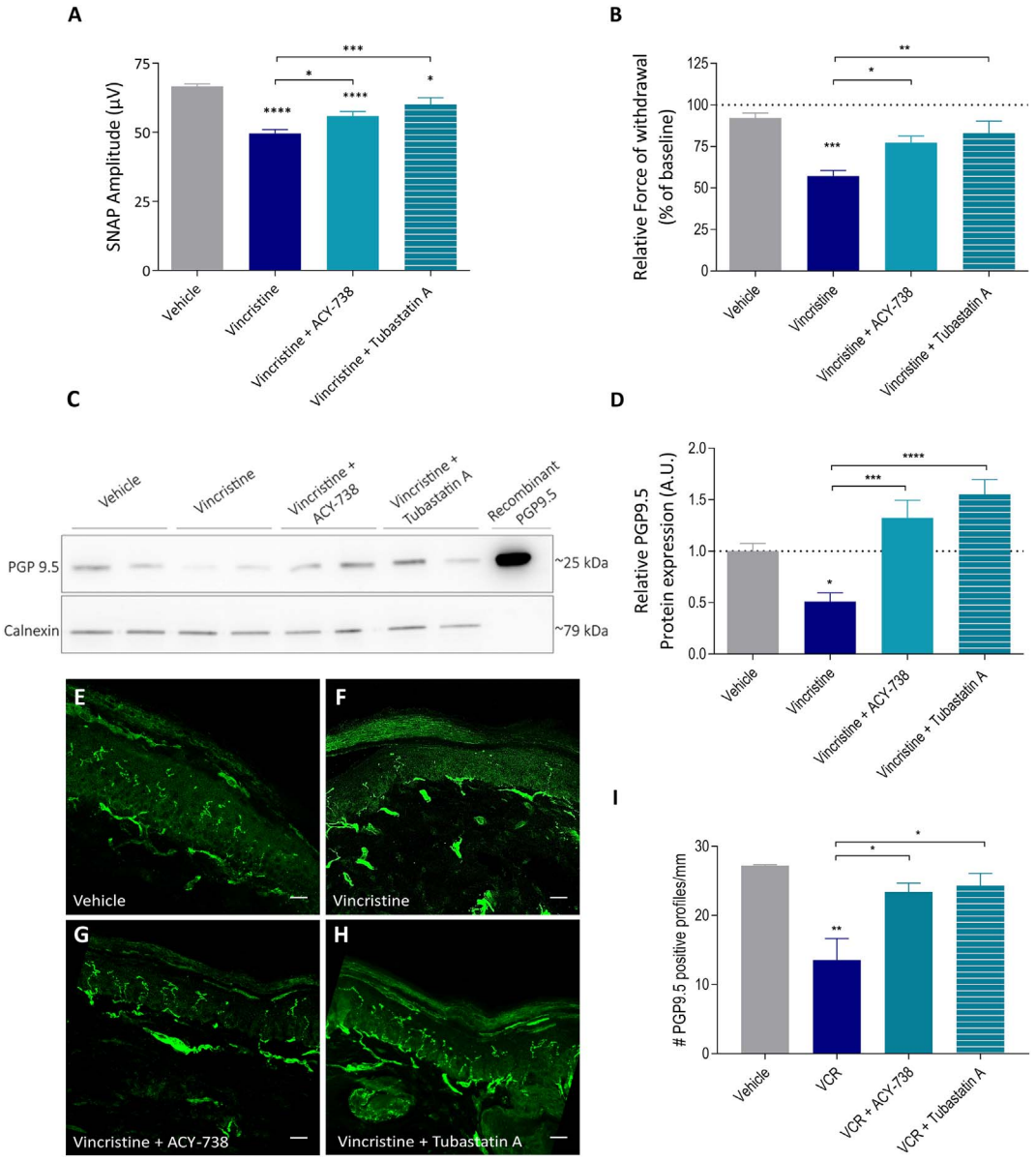

Fig. 1. HDAC6-inhibition protects against vincristine-induced sensory neurotoxicity in mice. **(A)** Characterization of the SNAP amplitude in the caudal nerve of mice treated with vehicle, vincristine alone, or in combination with an HDAC6 inhibitor (100mpk ACY-738 or 25 mg/kg/day Tubastatin A). **(B)** Assessment of the mechanical hypersensitivity by measuring the force required to provoke a reaction of the hind paw after 4 weeks of treatment. $N = 15–29$ animals per group. **(C)** Representative western blot of the pan-neuronal marker, protein gene product 9.5 (PGP9.5), in the skin isolated from animals after 4 weeks of treatment. $N = 9$ pooled from 3 experimental replicates. **(D)** Corresponding quantification of PGP9.5 protein expression. **(*E*-H)** Confocal images of PGP9.5 immunoreactive fibers in skin biopsies from mice after 4 weeks of treatment. Scale bar = 20 μm. **(I)** Quantification of the number of PGP9.5$^+$ fibers show that HDAC6 inhibition effectively preserves the innervation of the skin. A total of 30 sections, originating from 3 animals per treatment group, were used for quantification. Bars represent average ± SEM. Asterisk show significant differences with vehicle (above bar) or between vincristine-treated mice and the other groups. Two-Way ANOVA $^*p < 0.05$, $^{**}p < 0.01$, $^{***}p < 0.001$, $^{****}p < 0.0001$.

are in line with the pure sensory phenotype that we observe in these animals. Inhibition of HDAC6 in vincristine-treated mice significantly increased the levels of acetylated α-tubulin in the affected tissues, without modifying the expression of total α-tubulin (Fig. 2 and Supplemental Fig. S3). We obtained comparable results in tissues isolated from rats treated with vehicle, vincristine alone, or in combination with ACY-738 (Supplemental Figs. S4 and S5).

2.3. HDAC6 inhibition increases acetylated α-tubulin and preserves mitochondrial transport in DRG neurons treated with vincristine

In order to get mechanistic insights, we analyzed whether the increased levels of acetylated α-tubulin by HDAC6 inhibition could improve axonal transport in an *in vitro* system. We observed that HDAC6 inhibition increased the level of acetylated α-tubulin in neurites of cultured DRG neurons (Fig. 3). In contrast to our *in vivo* data, we could not detect a reduction in the α-tubulin acetylation level in cultured DRG neurons after treatment with vincristine alone (Fig. 3 and Supplemental Fig. S6). In order to test the effect on axonal transport of increasing acetylated α-tubulin through HDAC6 inhibition, we performed live cell imaging of mitochondrial transport in neurites of cultured DRG neurons. Viable mitochondria were fluorescently labelled after overnight exposure to vincristine alone (0.1 nM) or in the presence of either ACY-738 (1 nM) or Tubastatin A (1 μM). Vincristine significantly decreased the number of moving mitochondria along the neurites (− 60.4%), without affecting the number of stationary mitochondria (Fig. 4). In the presence of either one of the HDAC6 inhibitors, movement of mitochondria along DRG neurites was completely retained (Fig. 4). These

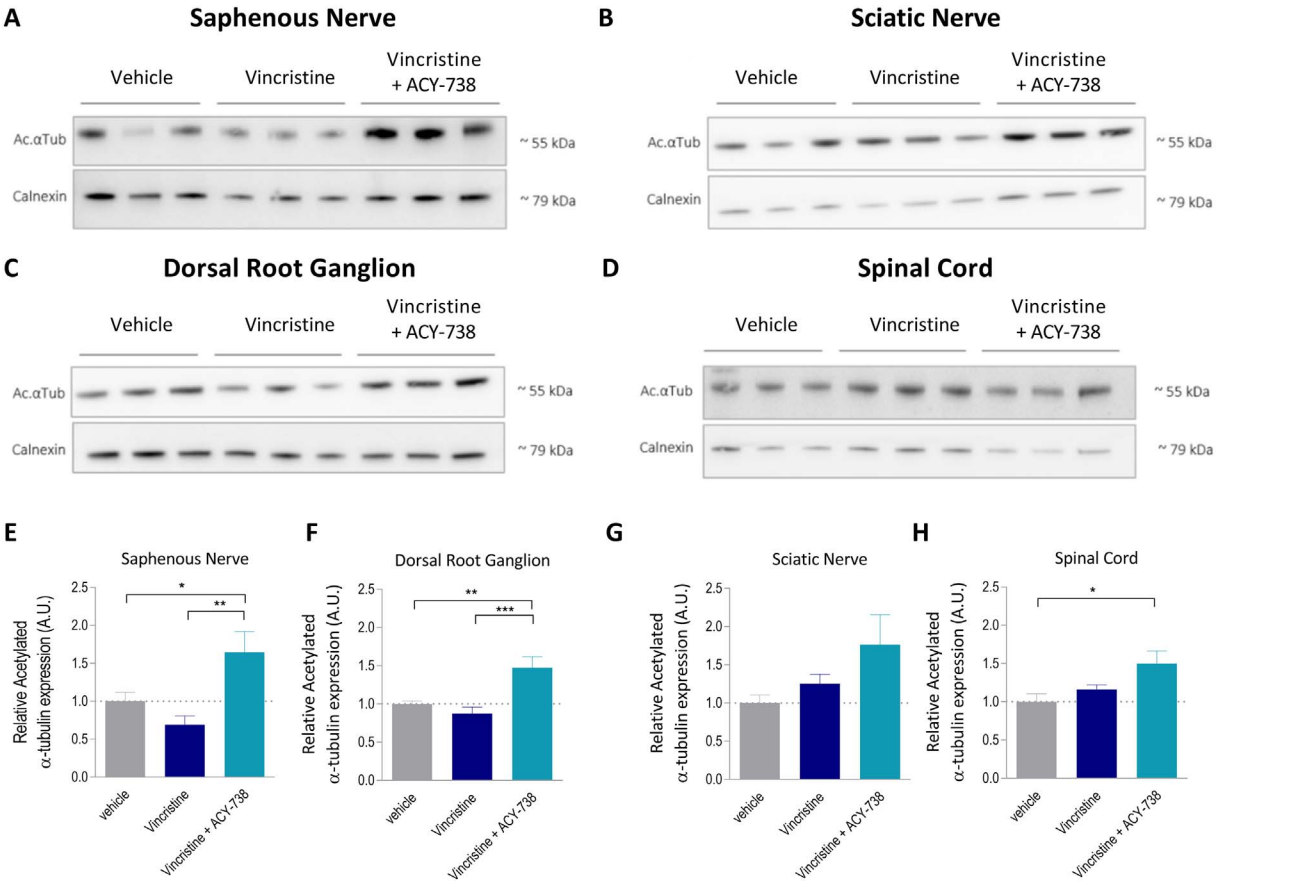

Fig. 2. HDAC6-inhibition restores the levels of acetylated α-tubulin in mice treated with vincristine. **(A–D)** Representative western blots from the saphenous nerve, sciatic nerve, DRGs and spinal cord, isolated from mice treated with vehicle, vincristine alone, or in combination with the HDAC6 inhibitor ACY-738 during a period of 4 weeks. **(E–H)** Quantification of the protein levels of acetylated α-tubulin in the saphenous nerve, DRGs, sciatic nerve and spinal cord. Calnexin was used to correct for unequal loading. Bars represent mean ± SEM. N = 9 animals per group pooled from 3 technical replicates. Two-way ANOVA revealed significant changes in α-tubulin acetylation where indicated with asterisks. *p < 0.05, **p < 0.01, ***$p < 0.001$.

results emphasize the importance of acetylated α-tubulin in cellular trafficking, and suggest that HDAC6-inhibition could restore vincristine-induced defects in axonal transport by increasing α-tubulin acetylation.

2.4. HDAC6 inhibition reduces tumor progression and prevents VIPN in a mouse model for acute lymphoblastic leukemia

In order to translate our findings into a clinically relevant application, the anti-cancer efficacy of vincristine should not be affected by the inhibition of HDAC6. Theoretically, it is possible that the positive effect of HDAC6 inhibition is due to a decrease of the efficacy of vincristine as both drugs interfere with microtubule dynamics. To investigate this, we used a humanized mouse model for T-cell acute lymphoblastic leukemia (ALL), a form of cancer commonly treated with vincristine (Soosay Raj et al., 2013). Male non-obese diabetic/severe combined immunodeficient gamma (NSG) mice were injected intravenously with acute lymphoblastic T-cells, isolated from a 4-year old patient. Tumor progression was analyzed through blood sampling and FACS sorting for human CD4-expressing tumor cells. In line with what was previously published, vincristine had a high efficacy against the expansion of human T-ALL cells (Douer, 2016). Moreover, tumor progression was almost completely repressed in animals co-treated with ACY-738 or with Tubastatin A (Fig. 5, A and D). This confirms previous reports that HDAC6 inhibition has a suppressive effect on tumor growth (Jones, 2013; Mishima et al., 2015; Santo et al., 2012; Vogl et al., 2015; Yee et al., 2016, 2014). Furthermore, vincristine-induced neurotoxicity was completely absent in animals co-treated with an HDAC6 inhibitor in comparison to animals receiving only vincristine, while the presence of ALL *per se* induced no neurological complications (Fig. 5, B and C and Supplemental Fig. S7). In contrast to what we observed before in wild type mice or rats, these immune-compromised animals presented with a more severe form of VIPN that was not limited to the sensory nerves, but also affected nerve conduction in the sciatic nerve. This was shown by the fact that CMAP amplitudes measured at the gastrocnemius muscle were also reduced after vincristine treatment (Fig. 5C). Inhibition of HDAC6 during chemotherapy completely prevented vincristine neurotoxicity, both in the sensory and motor nerves (Fig. 5, B and C). Taken together, our results strongly emphasize the potential of HDAC6 inhibitors as a therapy to treat VIPN as they do not only offer protection against neurotoxicity, but also exert additional benefits as an anti-cancer drug compared to vincristine alone.

3. Discussion

The development of a painful peripheral neuropathy is the dose-limiting side effect of a variety of anti-cancer therapies and a growing problem since cancer is becoming more and more a chronic disease (Cavaletti and Marmiroli, 2010; Phillips and Currow, 2010). Especially microtubule-interfering agents are well known to be neurotoxic and drastically affect the patients' quality of life (Gennery, 1985; LaPointe et al., 2013; Quasthoff and Hartung, 2002; Verstappen et al., 2003). Despite the fact that the mechanisms by which these drugs target cancer cells are well explored, the pathways causing the neuropathy remain incompletely understood. Here, we used rodent models to study the pathophysiology of chemotherapy-related neurotoxicity. Treatment

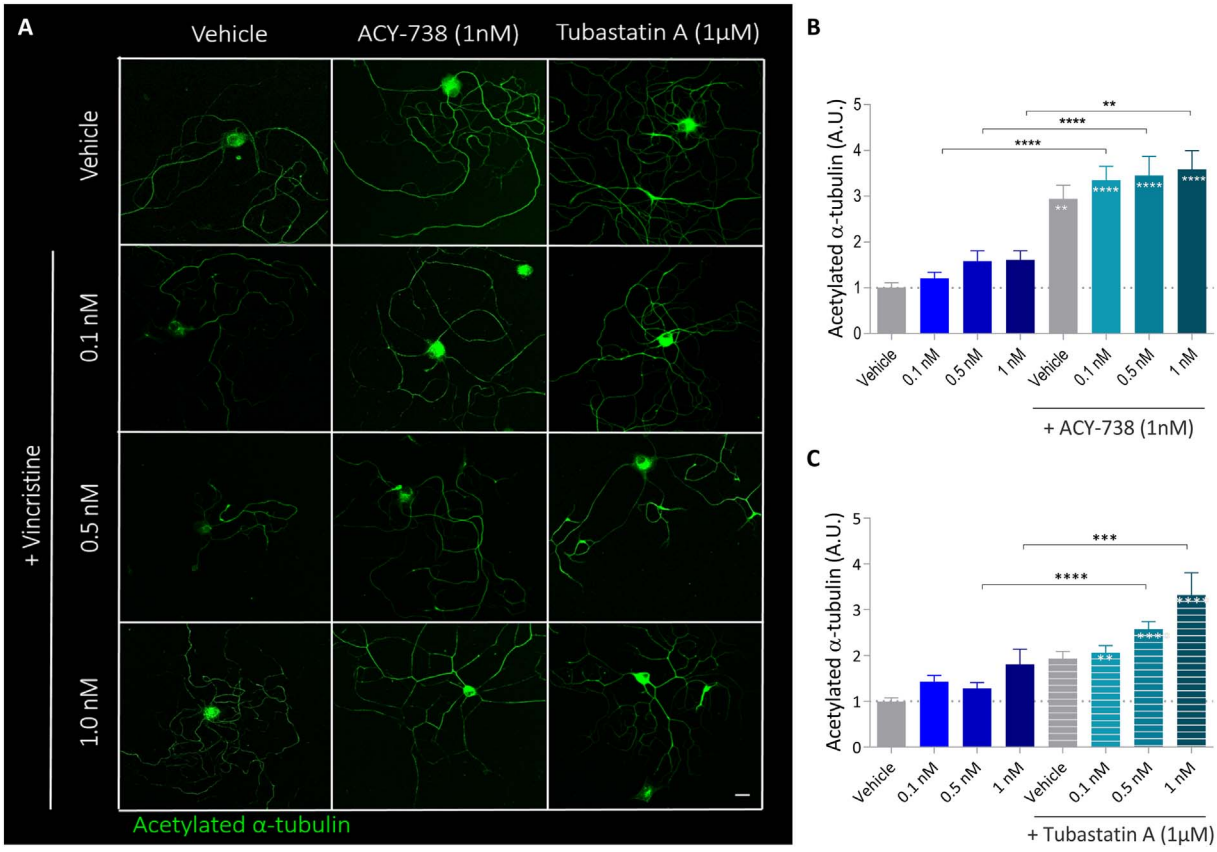

Fig. 3. The effects of vincristine and HDAC6-inhibition on acetylated α-tubulin in neurites of cultured DRG neurons. **(A)** Confocal images of DRG neurons stained for acetylated α-tubulin (green) and treated over night with different doses of vincristine in the absence or presence of the specific HDAC6 inhibitors Tubastatin A or ACY-738. Scare bar = 20 μm. **(B–C)** Quantification of the levels of acetylated α-tubulin along the neurites of DRG neurons treated with vincristine alone or in combination with the HDAC6 inhibitor, ACY-738 (1 nM) **(B)** or Tubastatin A (1 μM) **(C)**. Two-way ANOVA reveals significant differences in acetylated α-tubulin levels compared to vehicle treated neurons (white asterisk). Additionally, inhibition of HDAC6 significantly increased the acetylation of α-tubulin compared to the vincristine-treated condition (black asterisk). Bars represent the average ± SEM of 3 technical replicates. A total of 90–180 neurites were analyzed per condition. **p < 0.01, ***p < 0.001, ****p < 0.0001. (For interpretation of the references to colour in this figure legend, the reader is referred to the web version of this article.)

with vincristine resulted in a sensory axonopathy, comparable to the phenotype reported in humans (Boehmerle et al., 2014; Gennery, 1985; Grisold et al., 2012).

In contrast to hereditary diseases of the peripheral nervous system, the onset of neurotoxicity in CIPN only develops after the start of the anti-cancer treatment. This offers a major advantage and allows for early therapeutic intervention or even preventive treatments. Nevertheless, available strategies are primarily intended to alleviate the symptoms rather than to prevent the neuropathy from developing. This is at least in part due to a lack of mechanistic insights into CIPN. Our data suggest that disturbances in axonal transport could contribute to VIPN and we highlight the potential of HDAC6 inhibition as a therapeutic strategy to prevent vincristine-induced neurotoxicity. Indeed, co-treatment of rodents with HDAC6 inhibitors significantly reduced the severity of VIPN, both at the electrophysiological and at the behavioral level. We demonstrate that fast axonal transport of mitochondria was blocked by vincristine. Recently, Krukowski and colleagues suggested that mitochondrial dysfunction also contributes to cisplatin-induced peripheral neuropathy, a different form of CIPN (Krukowski et al., 2017). Using ACY-1083, another HDAC6-specific inhibitor, they were able to restore mitochondrial bioenergetics, mitochondrial axonal transport and the cisplatin-induced phenotype (Krukowski et al., 2017). Taken into account that vincristine inhibits the incorporation of αβ-tubulin heterodimers into microtubules (Jordan and Wilson, 2004; Jordanova et al., 2003), disturbances in microtubule dynamics could underlie the defects in axonal transport.

Tubulin is highly decorated with post-translational modifications to regulate microtubule dynamics. In a cell, there is a complex heterogeneity in microtubule function, each requiring a different degree of dynamicity. In order to organize the microtubule network, multiple combinations of post-translational modification form the so called 'tubulin code' (Janke and Chloë Bulinski, 2011). In the axon, microtubules are highly acetylated on lys-40 residues of α-tubulin, which has been shown to facilitate the docking of motor proteins (Reed et al., 2006) and to promote axonal transport (Dompierre et al., 2007). We did not observe a strong reduction in α-tubulin acetylation in cultured DRGs. However, it remains possible that vincristine alters the axonal tubulin code in DRG neurons by reducing acetylation only in the distal part of the axon. Indeed, vincristine inhibits the distal polymerization of microtubules, which is necessary for α-tubulin acetylation (Chakraborti et al., 2016; Janke and Chloë Bulinski, 2011). This points, together with the stocking-glove distribution observed in patients, towards VIPN as a form of "dying-back" neuropathy (Ravula et al., 2007), but needs to be further characterized. Inhibition of HDAC6 prevents deacetylation of microtubules, which keeps them in a polymerized state and therefore could have a protective effect against vincristine-induced alterations of the tubulin code. These preserved microtubules can keep serving as tracks for intracellular trafficking along the axon, counteracting the dying-back neuropathy.

In vivo, the degree of α-tubulin acetylation was mildly reduced after vincristine treatment exclusively in sensory tissues, such as the saphenous nerve and DRGs, but not in sciatic nerve or spinal cord. This correlates with the pure sensory phenotype observed in rodent models for VIPN (our data and (Boehmerle et al., 2014)). Inhibition of HDAC6

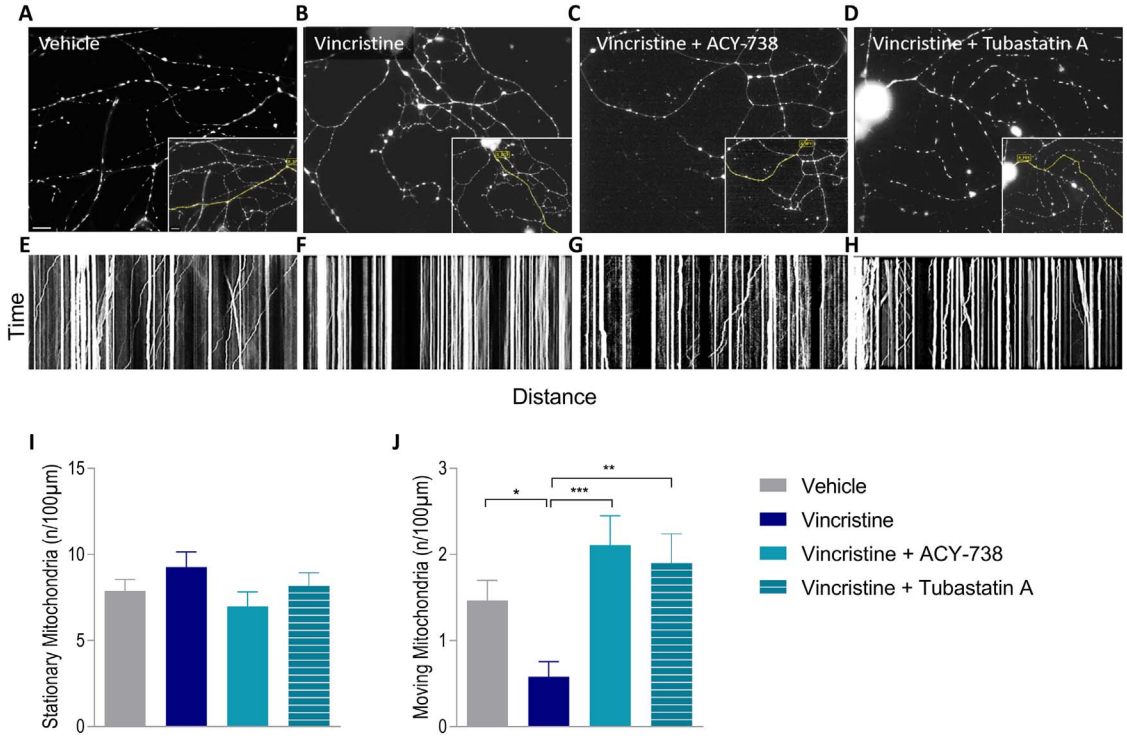

Fig. 4. HDAC6-inhibition rescues defects in axonal transport of mitochondria in DRG neurons treated with vincristine. **(A–D)** Representative images of DRG neurons in culture treated with vehicle, vincristine alone (0.1 nM) or in combination with an HDAC6 inhibitor (ACY-738, 1 nM or Tubastatin A, 1 μM). Viable mitochondria are labelled with MitoTracker-RED. Scale bars are 20 μm. **(E–H)** Corresponding kymographs, reconstituted from a live cell video of mitochondria within a single neurite, shown in the inserts of panel **A–D**. Stationary mitochondria are depicted as vertical lines, whereas moving mitochondria are illustrated by a skewed line. **(I, J)** Quantification of stationary and moving mitochondria along the neurite of a DRG neuron. Bars represent mean ± SEM of 6 experiments. A total of ≥ 30 DRG neurons per group were analyzed. Significant differences are indicated with asterisks. Two-Way ANOVA *$p < 0.05$, **$p < 0.01$, ***$p < 0.001$. (For interpretation of the references to colour in this figure legend, the reader is referred to the web version of this article.)

potently increased acetylated α-tubulin *in vitro* and in the affected sensory tissues from animals treated with vincristine. This could prevent the alterations in the dynamics of microtubules and could retain normal axonal transport along the sensory nerves. In turn, proper axonal transport ensures neuronal integrity and function, which could explain the positive effect on the SNAP amplitudes. In general, the amplitude is correlated with the number of functional axons within a nerve bundle (Van Asseldonk et al., 2003). As a consequence, a preventive treatment with HDAC6 inhibitors could preserve the intra-epidermal nerve fiber density, averting the symptoms of vincristine neurotoxicity during chemotherapy. Moreover, HDAC6 inhibition has also been shown to be effective in reversing neurotoxicity of cisplatin, another commonly used chemotherapeutic (Krukowski et al., 2017). Altogether, this implies that HDAC6 inhibition could be an efficient treatment strategy, applicable to multiple forms of CIPN.

Intensive research has been done either on the anti-cancer efficacy or on the neurological effects of vincristine, but little information is available on the combination of both disease aspects. This is crucial in order to translate any finding into a clinically relevant application, as neurological treatments should not interfere with the anti-cancer efficacy of chemotherapeutics. Therefore, it was essential to confirm that HDAC6-inhibition did not neutralize the positive effects of vincristine on tumor cells. To address this, we used a well-established cancer model for ALL (Agliano et al., 2008). The neurological phenotype induced by vincristine in these mice (NSG background) was more severe and not limited to sensory neurons, in contrast with immunocompetent mice on a C57BL6/J background. In general, sensory axons appear to be more vulnerable in comparison to motor axons. Although the mechanisms are largely unknown, differences in excitability, transcriptional profiles and axonal support have been suggested to underlie the diverse sensitivity of neuronal subtypes to stress situations (Brockington et al., 2013; Han and Smith, 2013; Hofmeijer et al., 2013). This could also explain the involvement of the motor axons in NSG mice, which were unaffected in immunocompetent rodents. In fact, Höke and Ray attribute the large variation between rodent models for CIPN to factors such as age and gender, as well as to the genetic background of different strains (Höke and Ray, 2014). In line with multiple studies that identified anti-proliferative effects of specific HDAC6 inhibitors towards cancer cellss (Huang et al., 2016; Jones, 2013; Mishima et al., 2015; North et al., 2017; Santo et al., 2012; Vogl et al., 2015; Yang et al., 2013; Yee et al., 2016, 2014), we observed that combining HDAC6 inhibitors with vincristine had an additive positive effect on tumor proliferation. This suggests that HDAC6 inhibition has its effect through a different mechanism compared to the vincristine effect on the reduction of tumor proliferation. Mounting evidence indicates that HDAC6 inhibitors are potent tumor suppressors through their effects on cell motility, oncogenic cell transformation, cellular stress response and/or tumorigenesis (reviewed in (Sakamoto and Aldana-Masangkay, 2011)). Furthermore, HDAC6 expression correlates with a poor prognosis in multiple forms of cancer (Hance et al., 2005; Manne et al., 2014; Park et al., 2015; Zhang et al., 2017). As such, the structurally related HDAC6 inhibitors Ricolinostat (ACY-1215) and Citarinostat (ACY-241) are currently being tested in Phase 2 clinical trials for the treatment of multiple myeloma (Santo et al., 2012; Yee et al., 2016, 2014). Taken together, HDAC6 is accepted as an anti-cancer target itself, though *via* its actions on other substrates than α-tubulin. These could include HSP90, cortactin, peroxiredoxins as well as a more general effect on inflammation, the protein-stress response and the ubiquitin-proteasome pathway (Sakamoto and Aldana-Masangkay, 2011; Van Helleputte et al., 2014). Therefore, the importance of HDAC6 inhibition as an add-on therapy to existing chemotherapies could by far exceed vincristine-based treatments alone.

In conclusion, we provide evidence that HDAC6 inhibitors, such as ACY-738 and Tubastatin A, are promising drugs for the treatment of

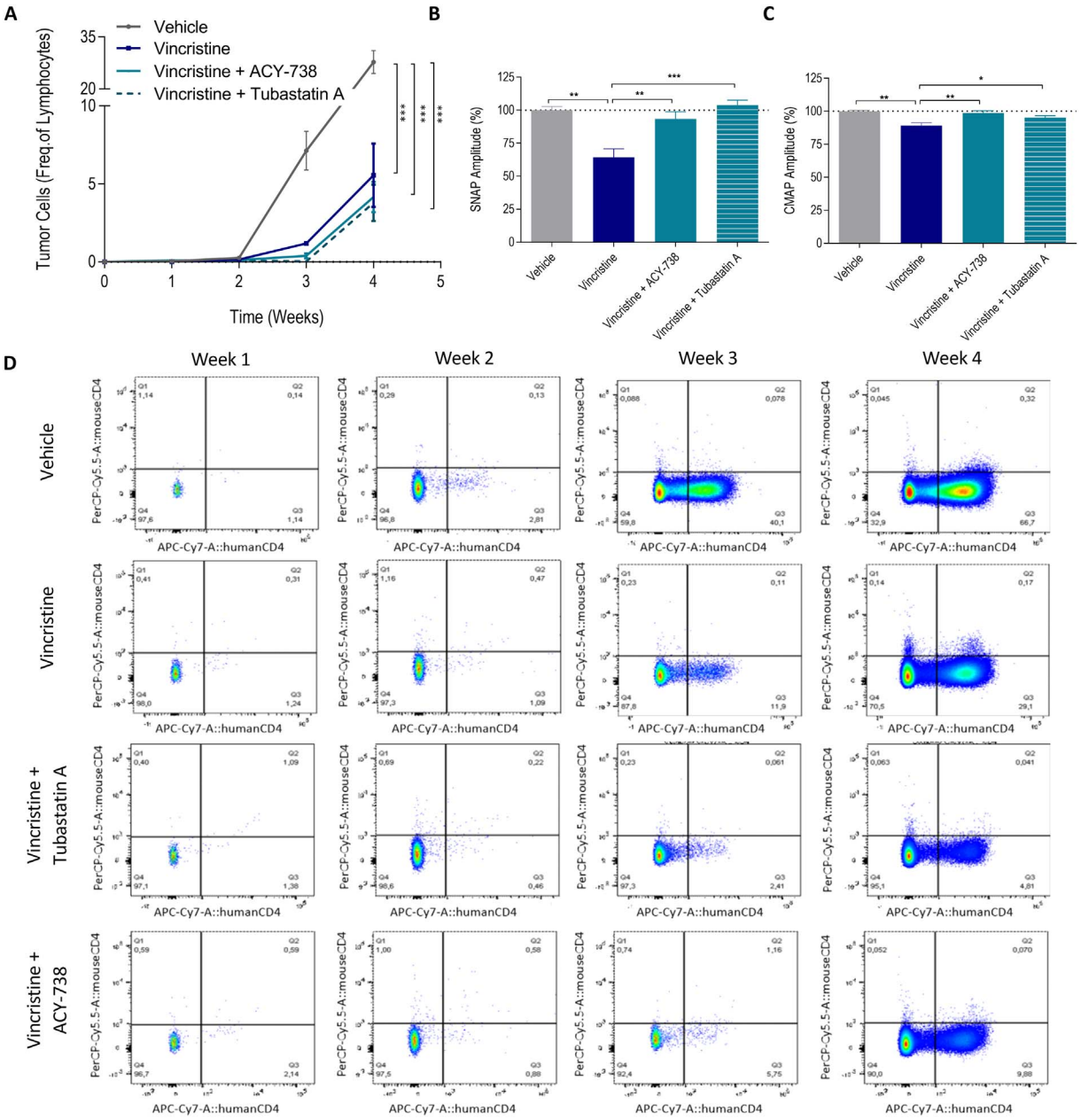

Fig. 5. HDAC6-inhibition inhibits tumor progression and prevents vincristine-induced neurotoxicity in a mouse model for T-cell ALL. **(A)** Quantification of tumor progression over time in sub-lethally irradiated mice injected with human CD4 expressing T-ALL cells. Animals were treated with weekly intraperitoneal (ip) injections of vehicle, vincristine alone, or in combination with an HDAC6 inhibitor (either ACY-738 or Tubastatin A) for a period of 4 weeks. **(D)** Representative plots obtained after FACS analysis of blood samples. **(B, C)** Determination of the neurological phenotype in mice 4 weeks after injection with human cancer cells. The sensory and motor phenotype was analyzed by determination of SNAP amplitude **(B)** and CMAP amplitude **(C)**, respectively. Graphs and bars represent mean values ± SEM. $N = 5$ per group and significance is indicated with asterisks. Two-Way ANOVA *$p < 0.05$, **$p < 0.01$, ****$p < 0.0001$.

VIPN. On one hand, suppression of HDAC6 has beneficial effects on the painful peripheral neuropathy in rodent models for VIPN, both on the electrophysiological and on the behavioral level. These effects correlate with a conservation of axonal transport, most likely mediated *via* an increase in α-tubulin acetylation, which could counteract the neuropathy and preserve the normal innervation of the skin. On the other hand, supplementing HDAC6 inhibitors to vincristine-based chemotherapy additionally reduced the proliferation of lymphoblastic T-cells, without affecting the positive protective effect against vincristine neurotoxicity. As a consequence, HDAC6 inhibitors in combination with classical chemotherapeutics could offer major advantages for the treatment of various types of cancers.

4. Material and methods

4.1. Animals and treatment strategies

Three to six month old male C57Bl6/J mice or six to eight week old male Sprague-Dawley (SD) rats were provided by the KU Leuven animal house or purchased from Envigo (Cambridgeshire, UK). All animals were housed according to the guidelines of the KU Leuven. Temperature (20–21 °C) and humidity (50–60%) were controlled and animals were kept on a 12 h light – 12 h dark cycle.

Vincristine sulfate (Tocris Bioscience, Bristol, UK) was dissolved in 0.9% NaCl and administered once a week *via* intraperitoneal (ip) injections for 3–4 consecutive weeks at a final dose of either 500 μg/kg or

300 μg/kg for mice and rats respectively. For oral delivery of ACY-738 (Acetylon Pharmaceuticals, Boston, USA), Teklad LM-485 (7912) sterilizable rodent diet (Envigo) containing 100 mg/kg ACY-738 was provided *ad libitum*. Tubastatin A (Asclepia, Destelbergen, Belgium) was dissolved at a concentration 50 mg/ml in DMSO and stored at − 20 °C. Aliquots were diluted in saline and administered daily ip at a dose of 25 mg/kg.

4.2. Electrophysiology

Motor and sensory nerve conduction studies were performed as described previously with some minor changes (d'Ydewalle et al., 2011). Rodents were anaesthetized under a 2.5 l/min oxygen flow containing 1.5–2% isoflurane and placed on a heating pad during the measurements in order to maintain the thermoregulation (37 ± 0.5 °C). Nerve conduction studies were performed using platinum coated sub-dermal needle electrodes (Technomed Europe, Maastricht, The Netherlands) and a Natus UltraPro S100 (Natus Medical Incorporated, Pleasanton, USA). Compound muscle action potentials (CMAPs) were determined by measuring the electrical response of the neuromuscular unit at the gastrocnemius muscle after stimulation of the sciatic nerve. An anode and cathode sub-dermal electrode were positioned proximal of the sciatic notch, 0.5 cm apart from each other, while the recording electrode was situated at the location where the gastrocnemius muscle reached its maximal diameter. A reference electrode was placed at the ankle of the animal. Sensory nerve action potentials (SNAPs) were recorded along the dorsal caudal nerve. The stimulating anode and cathode were placed at the tip of the tail, separated by 0.5 cm. The recording electrode measured the response 3 cm more proximally. The reference electrode was again positioned 0.5 cm proximal from the recording electrode. Grounding electrodes were positioned between the cathode and the recording electrode.

4.3. Mechanical sensitivity assay and Rotarod

Mice were placed in a 1000 cm^3, and rats in a 2000 cm^3 box with a mesh floor and were allowed to acclimatize for 20–30 min. In order to test the mechanical sensitivity, an electronic Von Frey anesthesiometer (IITC Life Science, Woodland Hills, USA) was used. In brief, a blunt probe with 0.8 mm tip diameter was placed on a spring that recorded the applied pressure in an automated manner. The investigator was trained to apply the Von Frey probe perpendicular to the middle of the hind paw while gradually increasing the applied pressure. As the spring was compressed, the maximal pressure to incite a reaction in the animal was recorded. A positive reaction could be the abrupt moving, flickering or licking of the paw. A total of 5 trials on the left and right hind paw was averaged to obtain the final threshold value for each animal. Motor coordination was analyzed with running wheel rotarod (Ugo Basile, Monvalle, Italy). Running velocity was gradually increased from 4 to 40 rotations per minute over a timespan of 300 s. Three consecutive trials, separated by one minute resting, were averaged per measurement.

4.4. Histological examination of neuromuscular junctions

Mice were euthanized with CO_2 followed by cervical dislocation. Gastrocnemius muscles were dissected, snap-frozen in liquid nitrogen-cooled isopentane and stored at − 80 °C. Twenty micron thick cryosections were fixed with 4% paraformaldehyde for 15 min and rinsed with PBS. Aspecific reactivity was blocked using 5% normal donkey serum (Sigma-Aldrich) in PBS-0.1% Triton X-100. Nerve axons were visualized after overnight incubation (4 °C) with antibodies directed against the pan-neuronal marker neurofilament light-chain conjugated to Alexa-488 (Cell Signaling Technologies; 1:500) and the presynaptic marker synaptophysin (Cell Signaling Technologies; 1:500). Next, sections were incubated with secondary antibody (anti-rabbit Alexa-488, 1:1000, Life Technologies) and simultaneously, the neuromuscular endplate was labelled with α-bungarotoxin conjugated to Alexa-555 (Life technologies; 1:500, 2 h at room temperature). At least 100 neuromuscular junctions were analyzed for innervation, as determined by colocalization of the neurofilaments light-chain/synaptophysin and the α-bungarotoxin labelling, on a Zeiss Axio Imager M1 microscope (Carl Zeiss) equipped with an AxioCam MRm3 camera (Carl Zeiss, Oberkochen, Germany).

4.5. Histological examination of skin biopsies

Skin biopsies were isolated from euthanized mice and post-fixed in 4% paraformaldehyde (Sigma-Aldrich) over night at 4 °C. Next, samples were immersed in decalcifying solution containing 15% Sucrose (Sigma-Aldrich), 10% ethylenediaminetetraacetic acid (E26282, Sigma-Aldrich) and 0.07% Glycerol (Sigma-Aldrich) in PBS and gently shaken over night at 4 °C. Skin Biopsies were cryoprotected over night in 20% sucrose in PBS and imbedded in O.C.T. compound (VWR). Fourteen micron thick sections were washed and permeabilized with PBS-0.3% Triton X-100. Aspecific binding was blocked with 5% bovine serum albumin (Sigma-Aldrich) for 1 h at room temperature. Polyclonal rabbit anti-human PGP9.5 (CL7756AP-S, Cederlane, Burlington, Canada) was used at a dilution of 1:800 to visualize nerve endings in skin biopsies (over night, 4 °C). Next, sections were incubated with secondary antibody (anti-rabbit Alexa-488, 1:1000, Life Technologies) and autofluorescence was reduced after a 3 min incubation with 1% Sudan Black B (Sigma-Aldrich) in 70% EtOH. Representative Confocal images were obtained on a Leica TCS SP8 confocal laser scanning microscope (Leica Microsystems, Wetzlar, Germany). A minimum of 10 sections was quantified per biopsy and samples of $n = 3$ mice were used per treatment condition. Three-dimensional representations were generated using the Leica Application Suite × software (LAS × 3.3.0, Leica Microsystems) from 50 plane *Z*-stacks through a 14 μm thick section. Scale bar = 50 μm.

4.6. DRG cultures

Mice were euthanized with CO_2 and dorsal root ganglia were isolated and kept in B27/Hibernate A medium (Gibco Life Technologies, Carlsbad, USA) supplemented with 0.5 mM L-glutamine (Gibco) and kept at 4 °C during the dissection. DRGs were transferred to B27/Hibernate A medium and heated to 37 °C before replacing the medium with B27/Hibernate A containing 2 mg/ml papain (Worthington Biochemical Corporation, Lakewood, NJ) activated with 0.5 mM EDTA and 1 mM L-cysteine (Thermo Fisher, Waltham, USA), for dissociation of the DRGs at 37 °C for 45 min. Next, the dissociation-medium was replaced with B27/Hibernate A medium and DRGs were thoroughly resuspended by pipetting up and down. DRG neurons were purified on a density gradient, consisting of 4 layers of 35%, 25%, 20% and 15% OptiPrep (Sigma-Aldrich), centrifuged for 15 min at 800 g without applying a centrifuge brake. Next, the upper 3 ml was discarded while the rest of the fractions were diluted in 5 ml B27/Hibernate A medium and the pellet was discarded. In a next step the cell-suspension was centrifuged at 500*g* for 4 min after which the supernatant was again centrifuged at a higher speed (3000*g*) for 4 min. Both cell pellets were combined and diluted in B27/Neurobasal A (Gibco) containing 10 ng/ml nerve growth factor 2.5 s (Millipore, Billerica, USA) and Pen/Strep (50 U/ml). Cells were seeded and allowed to attach for 1 h at 37 °C in a 5% CO_2 incubator. Next, B27/Neurobasal A growth medium was added and DRG neurons were allowed to grow overnight at 37 °C in 5% CO_2.

4.7. Axonal transport

Fast axonal transport was measured based on the trafficking of mitochondria along the axons of cultured DRG neurons as previously described (d'Ydewalle et al., 2011). In brief, viable mitochondria within

the DRG neurons were visualized using Mitotracker-RED (Life Technologies, Carlsbad, USA). DRG neuronal cultures were incubated with 50 nM Mitotracker-RED for 15 min at 37 °C in a 5% CO_2 incubator. After the medium was replaced, Mitotracker-RED was excited at 540 nm using a TILL Poly V light source (Till Photonics, Graefelfing, Germany) and image sequences were recorded (200 images at 1 Hz) onto a cooled CCD camera (PCO sensicam-QE) using TillVisION software. A heated gravity-fed perfusion system with HEPES buffer, containing 148 mM NaCl, 5 mM KCl, 0.1 mM $MgCl_2$·1.6 H_2O, 10 mM glucose, 10 mM HEPES and 2 mM $CaCl_2$·2.2 H_2O, was used to control the temperature (37 °C) during the experiment. Image analyses were performed with Igor Pro (Wavemetrics, Portland, USA) using custom-written routines as described before (Vanden Berghe et al., 2004). This software generates spatio-temporal maps, or kymographs, where stationary mitochondria appear as straight lines and moving mitochondria generate tilted lines. The numbers of stationary and moving mitochondria were calculated from these maps in a semi-automated manner by distinguishing straight and tilted lines on the kymographs. An average of at least 10 DRG neurons per condition was obtained and repeated for 3 experiments.

4.8. Immunofluorescence of DRG cultures

Cultured DRG neurons were fixed in 4% paraformaldehyde (Sigma-Aldrich) for 15 min before blocking with 5% normal donkey serum (Sigma-Aldrich) in PBS-0.1% Triton X-100 (Sigma-Aldrich). Primary antibodies were directed against acetylated α-tubulin (Sigma-Aldrich; 1:10,000) and the neuron-specific β_{III}-tubulin for counterstaining (Abcam; 1:10,000). Secondary antibodies were conjugated with Alexa-488 and Alexa-555, respectively (Life Technologies; 1:10,000). DRG neuronal cultures were incubated with the antibodies for 1 h at room temperature. Fluorescent images were obtained using an AxioVision (version 4.8, Carl Zeiss) and analysis was performed using FIJI (NIH) with the Bioformats plugin. An average was taken of 3 repeated experiments with 30–60 pictures analyzed per condition and per experiment. Representative images were acquired on a Leica TCS SP8 confocal laser scanning microscope (Leica Microsystems).

4.9. Western blot

Tissues were homogenized in RIPA buffer complemented with a protease inhibitor cocktail (Roche, Bazel, Switzerland) using Lysing Matrix D beads (MP Biomedicals, Illkirch Cedex, France) and a MagNA Lyser instrument (Roche). The following primary antibodies were diluted in 5% blocking buffer: rabbit anti-HDAC6 (Cell Signaling Technologies; 1:250, overnight, RT), rabbit anti-PGP9.5 (Millipore; 1:1000, overnight, 4 °C), mouse anti-alpha-tubulin (Sigma-Aldrich; 1:10,000, overnight, 4 °C), mouse anti-acetylated alpha-tubulin (Cell Signaling Technologies; 1:5000, overnight, 4 °C) and rabbit anti-calnexin (Enzo Life Sciences; 1:2000, 1 h, RT). Secondary antibodies conjugated with horseradish peroxidase (Dako; 1:5000, 1 h, RT) were used prior to detection with ECL substrate (Life Technologies) with a LAS 4000 Image Analyser (GE Healthcare, Little Chalfont, UK). Luminescent signals were analyzed with ImageQuant TL software (GE Healthcare). Signals were normalized to calnexin to correct for unequal loading.

4.10. Xenograft model and flow cytometry

Human acute lymphoblastic T-cells (CCRF-CEM, ATCC®-CCL-119™) were purchased from American Type Culture Collection (ATCC, University Boulevard Manassas, USA) and cultured in RPMI-1640 medium (Gibco) supplemented with 10% fetal bovine serum (Gibco). Five hundred thousand cells were resuspended in PBS and injected intravenously in 8–12 week old NOD.Cg-Prkdc^{scid}Il2^{tm1Wjl}/Szj (NSG) mice (bred in house from stocks originally purchased from The Jackson Laboratories Bar Harbor, USA) 24 h after sublethal irradiation (2.5 Gy to the whole body). These animals received the same treatment with vincristine and/or Tubastatin A as described above for the VIPN mouse model. For practical reasons, we opted for daily ip injections with ACY-738 (Acetylon Pharmaceuticals) instead of oral delivery. ACY-738 was dissolved in DMSO at a stock concentration of 6 mg/ml. Stock solutions were diluted in 5% dextrose (Sigma-Aldrich, St. Louis, USA) to reach a final dose of 25 mg/kg. Peripheral blood was collected *via* submandibular bleeding. Following red blood cell lysis (0.83% NH_4Cl in 0.01 M Tris-HCl, pH 7.2), cells were stained with conjugated antibodies directed against the following markers (eBioscience, Buckinghamshire, UK): human CD3 (clone SK7), human CD4 (clone RPA-T4) and mouse CD4 (clone RM4-5). The number of human $CD4^+$ cells within the cell population gated as lymphocytes (based on the forward and side scatter values) were determined by flow cytometry using a BD FACSCanto II (BD Bioscience, Buckinghamshire, UK). Data were analyzed using the FlowJo V10.1 software (Tree Star Inc., Oregon, USA). Human $CD4^+$ cells were plotted on the x-axis *versus* the mouse $CD4^+$ cells on the y-axis. Tumor cells are represented by the human$CD4^+$/mouse$CD4^-$ population, denoted in Q3.

4.11. Statistics

All statistics were performed using GraphPad Prism 7.02 (GraphPad Software Inc., San Diego, USA). Unless otherwise specified, statistical significance was analyzed *via* 2-way ANOVA grouped test. The Bonferroni test was applied to correct for multiple testing. As appropriate, $p < 0.05$ was set as significance level.

4.12. Study approval

All procedures were conducted in accordance to the ethical standards for experiments on animals established and approved by the Animal Ethics Committee of the KU Leuven. Experiments were conducted under the ethical committee documents P182-2012 and P029-2014.

Supplementary data to this article can be found online at https://doi.org/10.1016/j.nbd.2017.11.011.

Acknowledgements

This work was supported by grants from the Fund for Scientific Research Flanders (FWO G.0920.15), the Belgian government (Interuniversity Attraction Poles of the Belgian Federal Science Policy Office (P7/16)), the Association Belge contre les Maladies neuro-Musculaires (ABMM), the Muscular Dystrophy Association (MDA295317), the European Community's Health Seventh Framework Programme (FP7/2007-2013 under grant agreement 259867) and NIH (NS079183). PVD, WR and LVDB are supported by the 'Opening the Future' Fund (KU Leuven). W.R. is supported through the E. von Behring Chair for Neuromuscular and Neurodegenerative Disorders and the European Research Council under the European's Seventh Framework Programme (FP7/2007-2013)/ ERC grant agreement n° 340429. LVH is supported by the 'Agency for Innovation by Science and Technology in Flanders' (IWT-Vlaanderen). PVD holds a clinical investigatorship of FWO-Vlaanderen. The authors declare no conflict of interest.

References

Agliano, A., Martin-Padura, I., Mancuso, P., Marighetti, P., Rabascio, C., Pruneri, G., Shultz, L.D., Bertolini, F., 2008. Human acute leukemia cells injected in NOD/LtSz-scid/IL-2Rγ null mice generate a faster and more efficient disease compared to other NOD/scid-related strains. Int. J. Cancer 123, 2222–2227. http://dx.doi.org/10.1002/ijc.23772.

Almeida-Souza, L., Timmerman, V., Janssens, S., 2011. Microtubule dynamics in the peripheral nervous system: a matter of balance. BioArchitecture 1, 267–270. http://

dx.doi.org/10.4161/bioa.1.6.19198.
Baron, R., 2006. Mechanisms of disease: neuropathic pain - a clinical perspective. Nat. Clin. Pract. Neurol. 2, 95–106. http://dx.doi.org/10.1038/ncpneuro0113.
Benoy, V., d'Ydewalle, C., Van Den Berghe, P., Van Damme, P., Kozikowski, A.P., Robberecht, W., Van Den Bosch, L., 2015. Therapeutic potential of selective inhibition of histone deacetylase 6 (HDAC6) in different froms of CMT2. In: Journal of the Peripheral Nervous System, pp. 103–104. http://dx.doi.org/10.1111/jns.12129.
Benoy, V., Vanden Berghe, P., Jarpe, M., Van Damme, P., Robberecht, W., Van Den Bosch, L., 2016. Development of improved HDAC6 inhibitors as pharmacological therapy for axonal Charcot–Marie–Tooth disease. Neurotherapeutics. http://dx.doi.org/10.1007/s13311-016-0501-z.
Bobylev, I., Joshi, A.R., Barham, M., Neiss, W.F., Lehmann, H.C., 2017. Depletion of Mitofusin-2 causes mitochondrial damage in cisplatin-induced neuropathy. Mol. Neurobiol. 1–9. http://dx.doi.org/10.1007/s12035-016-0364-7.
Boehmerle, W., Huehnchen, P., Peruzzaro, S., Balkaya, M., Endres, M., 2014. Electrophysiological, behavioral and histological characterization of paclitaxel, cisplatin, vincristine and bortezomib-induced neuropathy in C57Bl/6 mice. Sci. Rep. 4, 6370. http://dx.doi.org/10.1038/srep06370.
Brockington, A., Ning, K., Heath, P.R., Wood, E., Kirby, J., Fusi, N., Lawrence, N., Wharton, S.B., Ince, P.G., Shaw, P.J., 2013. Unravelling the enigma of selective vulnerability in neurodegeneration: motor neurons resistant to degeneration in ALS show distinct gene expression characteristics and decreased susceptibility to excitotoxicity. Acta Neuropathol. 125, 95–109. http://dx.doi.org/10.1007/s00401-012-1058-5.
Butler, K.V., Kalin, J., Brochier, C., Vistoli, G., Langley, B., Kozikowski, A.P., 2010. Rational design and simple chemistry yield a superior, neuroprotective HDAC6 inhibitor, tubastatin A. J. Am. Chem. Soc. 132, 10842–10846. http://dx.doi.org/10.1021/ja102758v.
Cashman, C.R., Höke, A., 2015. Mechanisms of distal axonal degeneration in peripheral neuropathies. Neurosci. Lett. 596, 33–50. http://dx.doi.org/10.1016/j.neulet.2015.01.048.
Cavaletti, G., Marmiroli, P., 2010. Chemotherapy-induced peripheral neurotoxicity. Nat. Rev. Neurol. 6 (12), 657–666. http://dx.doi.org/10.1038/nrneurol.2010.160. Epub 2010 Nov 9 (Dec).
Cavaletti, G., Alberti, P., Frigeni, B., Piatti, M., Susani, E., 2011. Chemotherapy-induced neuropathy. Curr. Treat. Options Neurol. http://dx.doi.org/10.1007/s11940-010-0108-3.
Chakraborti, S., Natarajan, K., Curiel, J., Janke, C., Liu, J., 2016. The emerging role of the tubulin code: from the tubulin molecule to neuronal function and disease. Cytoskeleton. http://dx.doi.org/10.1002/cm.21290.
Conde, C., Caceres, A., Cáceres, A., 2009. Microtubule assembly, organization and dynamics in axons and dendrites. Nat. Rev. Neurosci. 10, 319–332. http://dx.doi.org/10.1038/nrn2631.
De Vos, K.J., Hafezparast, M., 2017. Neurobiology of axonal transport defects in motor neuron diseases: opportunities for translational research? Neurobiol. Dis. http://dx.doi.org/10.1016/j.nbd.2017.02.004.
Dompierre, J.P., Godin, J.D., Charrin, B.C., Cordelières, F.P., King, S.J., Humbert, S., Saudou, F., Cordelieres, F.P., King, S.J., Humbert, S., Saudou, F., 2007. Histone deacetylase 6 inhibition compensates for the transport deficit in Huntington's disease by increasing tubulin acetylation. J. Neurosci. 27, 3571–3583. http://dx.doi.org/10.1523/JNEUROSCI.0037-07.2007.
Douer, D., 2016. Efficacy and safety of vincristine sulfate liposome injection in the treatment of adult acute lymphocytic leukemia. Oncologist 21, 840–847. http://dx.doi.org/10.1634/theoncologist.2015-0391.
Gennery, B.A., 1985. Vincristine neurotoxicity. Lancet (Lond.) 2, 385.
Grisold, W., Cavaletti, G., Windebank, A.J., 2012. Peripheral neuropathies from chemotherapeutics and targeted agents: diagnosis, treatment, and prevention. Neuro-Oncology 14. http://dx.doi.org/10.1093/neuonc/nos203.
Grozinger, C.M., Hassig, C.A., Schreiber, S.L., 1999. Three proteins define a class of human histone deacetylases related to yeast Hda1p. Biochemistry 96, 4868–4873.
Han, Y., Smith, M.T., 2013. Pathobiology of cancer chemotherapy-induced peripheral neuropathy (CIPN). Front. Pharmacol. http://dx.doi.org/10.3389/fphar.2013.00156.
Hance, K.W., Anderson, W.F., Devesa, S.S., Young, H.A., Levine, P.H., 2005. Trends in inflammatory breast carcinoma incidence and survival: the surveillance, epidemiology, and end results program at the National Cancer Institute. J. Natl. Cancer Inst. 97, 966–975. http://dx.doi.org/10.1093/jnci/dji172.
Hofmeijer, J., Franssen, H., van Schelven, L.J., van Putten, M.J.A.M., 2013. Why are sensory axons more vulnerable for ischemia than motor axons? PLoS One 8. http://dx.doi.org/10.1371/journal.pone.0067113.
Höke, A., Ray, M., 2014. Rodent models of chemotherapy-induced peripheral neuropathy. ILAR J. 54, 273–281. http://dx.doi.org/10.1093/ilar/ilt053.
Holzbaur, Erika L.F., Scherer, Steven S., 2011. Microtubules, axonal transport, and neuropathy. N. Engl. J. Med. 365, 2330–2332. http://dx.doi.org/10.1056/NEJMcibr1112481.Microtubules.
Huang, P., Almeciga-Pinto, I., Jarpe, M., van Duzer, J.H., Mazitschek, R., Yang, M., Jones, S.S., Quayle, S.N., Huang, P., Almeciga-Pinto, I., Jarpe, M., van Duzer, J.H., Mazitschek, R., Yang, M., Jones, S.S., Quayle, S.N., 2016. Selective HDAC inhibition by ACY-241 enhances the activity of paclitaxel in solid tumor models. Oncotarget 8, 2694–2707. http://dx.doi.org/10.18632/oncotarget.13738.
Hubbert, C., Guardiola, A., Shao, R., Kawaguchi, Y., Ito, A., Nixon, A., Yoshida, M., Wang, X.-F.F., Yao, T.-P.P., 2002. HDAC6 is a microtubule-associated deacetylase. Nature 417, 455–458. http://dx.doi.org/10.1038/417455a417455a [pii].
Jaggi, A.S., Singh, N., 2012. Mechanisms in cancer-chemotherapeutic drugs-induced peripheral neuropathy. Toxicology. http://dx.doi.org/10.1016/j.tox.2011.10.019.
Janke, C., Chloë Bulinski, J., 2011. Post-translational regulation of the microtubule cytoskeleton: mechanisms and functions. Nat. Rev. Mol. Cell Biol. 12, 773–786. http://dx.doi.org/10.1038/nrm3227.
Jochems, J., Boulden, J., Lee, B.G., Blendy, J.A., Jarpe, M., Mazitschek, R., Van Duzer, J.H., Jones, S., Berton, O., 2014. Antidepressant-like properties of novel HDAC6-selective inhibitors with improved brain bioavailability. Neuropsychopharmacology 39, 389–400. http://dx.doi.org/10.1038/npp.2013.207npp2013207. [pii].
Jones, S.S., 2013. ACY-1215, a first-in-class selective inhibitor of HDAC6, demonstrates significant synergy with immunomodulatory drugs (IMiDs) in preclinical models of multiple myeloma (MM). Blood 122, 1952.
Jordan, M.M.A.M.A., Wilson, L., 2004. Microtubules as a target for anticancer drugs. Nat. Rev. Cancer 4, 253–265. http://dx.doi.org/10.1038/nrc1317.
Jordanova, A., De Jonghe, P., Boerkoel, C.F., Takashima, H., De Vriendt, E., Ceuterick, C., Martin, J.J., Butler, I.J., Mancias, P., Papasozomenos, S.C., Terespolsky, D., Potocki, L., Brown, C.W., Shy, M., Rita, D.A., Tournev, I., Kremensky, I., Lupski, J.R., Timmerman, V., 2003. Mutations in the neurofilament light chain gene (NEFL) cause early onset severe Charcot-Marie-Tooth disease. Brain 126, 590–597. http://dx.doi.org/10.1093/brain/awg059.
Kannarkat, G., Lasher, E.E., Schiff, D., 2007. Neurologic complications of chemotherapy agents. Curr. Opin. Neurol. 20, 719–725. http://dx.doi.org/10.1097/WCO.0b013e3282f1a06e.
Krukowski, K., Ma, J., Golonzhka, O., Laumet, G.O., Gutti, T., van Duzer, J.H., Mazitschek, R., Jarpe, M.B., Heijnen, C.J., Kavelaars, A., 2017. HDAC6 inhibition effectively reverses chemotherapy-induced peripheral neuropathy. Pain 1. http://dx.doi.org/10.1097/j.pain.0000000000000893.
LaPointe, N.E., Morfini, G., Brady, S.T., Feinstein, S.C., Wilson, L., Jordan, M.A., 2013. Effects of eribulin, vincristine, paclitaxel and ixabepilone on fast axonal transport and kinesin-1 driven microtubule gliding: implications for chemotherapy-induced peripheral neuropathy. Neurotoxicology 37, 231–239. http://dx.doi.org/10.1016/j.neuro.2013.05.008.
Lawson, J.L.D., Carazo Salas, R.E., 2013. Microtubules: greater than the sum of the parts. Biochem. Soc. Trans. 41, 1736–1744. http://dx.doi.org/10.1042/BST20130239.
Majithia, N., Loprinzi, C.L., Smith, T.J., 2016. New practical approaches to chemotherapy-induced neuropathic pain: prevention, assessment and treatment. Oncology (Williston Park) 30, 1–13.
Manne, R.K., Madu, C.S., Talla, H.V., 2014. Maxillary sporadic Burkitt's lymphoma associated with neuro-orbital involvement in an Indian male. Contemp. Clin. Dent. 5, 231–235. http://dx.doi.org/10.4103/0976-237X.132357.
Mishima, Y., Santo, L., Eda, H., Cirstea, D., Nemani, N., Yee, A.J., O'Donnell, E., Selig, M.K., Quayle, S.N., Arastu-Kapur, S., Kirk, C., Boise, L.H., Jones, S.S., Raje, N., 2015. Ricolinostat (ACY-1215) induced inhibition of aggresome formation accelerates carfilzomib-induced multiple myeloma cell death. Br. J. Haematol. 169, 423–434. http://dx.doi.org/10.1111/bjh.13315.
North, B.J., Almeciga-Pinto, I., Tamang, D., Yang, M., Jones, S.S., Quayle, S.N., 2017. Enhancement of pomalidomide anti-tumor response with ACY-241, a selective HDAC6 inhibitor. PLoS One 12. http://dx.doi.org/10.1371/journal.pone.0173507.
Park, S.B., Goldstein, D., Krishnan, A.V., Lin, C.S.-Y., Friedlander, M.L., Cassidy, J., Koltzenburg, M., Kiernan, M.C., 2013. Chemotherapy-induced peripheral neurotoxicity: a critical analysis. CA Cancer J. Clin. 63, 419–437. http://dx.doi.org/10.3322/caac.21204.
Park, Y., Lee, K.S., Park, S.Y., Kim, J.H., Kang, E.Y., Kim, S.W., Eom, K.Y., Kim, J.S., Kim, I.A., 2015. Breast cancer potential prognostic value of histone deacetylase 6 and acetylated heat-shock protein 90 in early-stage breast cancer. J. Breast Cancer 18, 249–255. http://dx.doi.org/10.4048/jbc.2015.18.3.249.
Phillips, J.L., Currow, D.C., 2010. Cancer as a chronic disease. Collegian 17, 47–50. http://dx.doi.org/10.1016/j.colegn.2010.04.007.
Podratz, J.L., Lee, H., Knorr, P., Koehler, S., Forsythe, S., Lambrecht, K., Arias, S., Schmidt, K., Steinhoff, G., Yudintsev, G., Yang, A., Trushina, E., Windebank, A., 2017. Cisplatin induces mitochondrial deficits in *Drosophila* larval segmental nerve. Neurobiol. Dis. 97, 60–69. http://dx.doi.org/10.1016/j.nbd.2016.10.003.
Prior, R., Van Helleputte, L., Benoy, V., Van Den Bosch, L., 2017. Defective axonal transport: A common pathological mechanism in inherited and acquired peripheral neuropathies. pii: S0969. Neurobiol. Dis. 105, 300–320. http://dx.doi.org/10.1016/j.nbd.2017.02.009. Epub 2017 Feb 24 (Sep).
Quasthoff, S., Hartung, H.P., 2002. Chemotherapy-induced peripheral neuropathy. J. Neurol. 249, 9–17. http://dx.doi.org/10.1007/PL00007853.
Ravula, S.K., Wang, M.S., McClain, M.A., Asress, S.A., Frazier, B., Glass, J.D., 2007. Spatiotemporal localization of injury potentials in DRG neurons during vincristine-induced axonal degeneration. Neurosci. Lett. 415, 34–39. http://dx.doi.org/10.1016/j.neulet.2007.01.009.
Reed, N.A., Cai, D., Blasius, T.L., Jih, G.T., Meyhofer, E., Gaertig, J., Verhey, K.J., 2006. Microtubule acetylation promotes kinesin-1 binding and transport. Curr. Biol. 16, 2166–2172. http://dx.doi.org/10.1016/j.cub.2006.09.014.
Sakamoto, K.M., Aldana-Masangkay, G.I., 2011. The role of HDAC6 in cancer. J Biomed Biotechnol 2011, 875824. http://dx.doi.org/10.1155/2011/875824.
Santo, L., Hideshima, T., Kung, A.L., Tseng, J.C., Tamang, D., Yang, M., Jarpe, M., Van Duzer, J.H., Mazitschek, R., Ogier, W.C., Cirstea, D., Rodig, S., Eda, H., Scullen, T., Canavese, M., Bradner, J., Anderson, K.C., Jones, S.S., Raje, N., 2012. Preclinical activity, pharmacodynamic, and pharmacokinetic properties of a selective HDAC6 inhibitor, ACY-1215, in combination with bortezomib in multiple myeloma. Blood 119, 2579–2589. http://dx.doi.org/10.1182/blood-2011-10-387365.
Schneider, B.P., Hershman, D.L., Loprinzi, C., 2015. Symptoms: chemotherapy-induced peripheral neuropathy. Adv. Exp. Med. Biol. 862, 77–87. http://dx.doi.org/10.1007/978-3-319-16366-6_6.
Seretny, M., Currie, G.L., Sena, E.S., Ramnarine, S., Grant, R., Macleod, M.R., Colvin, L.A., Fallon, M., 2014. Incidence, prevalence, and predictors of chemotherapy-induced peripheral neuropathy: a systematic review and meta-analysis. Pain 155, 2461–2470. http://dx.doi.org/10.1016/j.pain.2014.09.020.

Shen, S., Benoy, V., Bergman, J.A., Kalin, J.H., Frojuello, M., Vistoli, G., Haeck, W., Van Den Bosch, L., Kozikowski, A.P., 2016. Bicyclic-capped histone deacetylase 6 inhibitors with improved activity in a model of axonal Charcot-Marie-Tooth disease. ACS Chem. Neurosci. 7, 240–258. http://dx.doi.org/10.1021/acschemneuro.5b00286.

Silva, A., Wang, Q., Wang, M., Ravula, S.K., Glass, J.D., 2006. Evidence for direct axonal toxicity in vincristine neuropathy. J. Peripher. Nerv. Syst. 11, 211–216. http://dx.doi.org/10.1111/j.1529-8027.2006.0090.x.

Soosay Raj, T.A., Smith, A.M., Moore, A.S., 2013. Vincristine sulfate liposomal injection for acute lymphoblastic leukemia. Int. J. Nanomedicine. http://dx.doi.org/10.2147/IJN.S54657.

Stanton, R.A., Gernert, K.M., Nettles, J.H., Aneja, R., 2011. Drugs that target dynamic microtubules: a new molecular perspective. Med. Res. Rev. 31, 443–481. http://dx.doi.org/10.1002/med.20242.

Van Asseldonk, J.T.H., Van den Berg, L.H., Van den Berg-Vos, R.M., Wieneke, G.H., Wokke, J.H.J., Franssen, H., 2003. Demyelination and axonal loss in multifocal motor neuropathy: distribution and relation to weakness. Brain 126, 186–198. http://dx.doi.org/10.1093/brain/awg019.

Van Helleputte, L., Benoy, V., Van Den Bosch, L., 2014. The role of histone deacetylase 6 (HDAC6) in neurodegeneration. Res. Rep. Biol. 5, 1–13. http://dx.doi.org/10.2147/RRB.S35470.

Vanden Berghe, P., Hennig, G.W., Smith, T.K., 2004. Characteristics of intermittent mitochondrial transport in guinea pig enteric nerve fibers. Am. J. Physiol. Gastrointest. Liver Physiol. 286, G671–82. http://dx.doi.org/10.1152/ajpgi.00283.2003.

Verstappen, C.C.P., Heimans, J.J., Hoekman, K., Postma, T.J., 2003. Neurotoxic complications of chemotherapy in patients with cancer: clinical signs and optimal management. Drugs 63, 1549–1563. http://dx.doi.org/10.2165/00003495-200363150-00003.

Vogl, D.T., Raje, N.S., Jagannath, S., Richardson, P.G., Hari, P., Orlowski, R.Z., Supko, J., Tamang, D., Jones, S.S., Wheeler, C., Markelewicz, R.J., Lonial, S., 2015. Ricolinostat (ACY-1215), the first selective HDAC6 inhibitor, in combination with bortezomib and dexamethasone in patients with relapsed or relapsed-and-refractory multiple myeloma: phase 1b results (ACY-100 study). Blood 126, 1827.

Yang, M., Tamang, D., Jones, S.S., Di, L., 2013. Large-scale cancer cell line screening with a novel and selective HDAC-6 inhibitor (ACY-1215) identifies candidate predictive biomarkers for breast cancer. In: Proceedings of the 104th Annual Meeting of the American Association for Cancer Research. Cancer Res. 73 AACR, Washington, DC. Philadelphia (PA). http://dx.doi.org/10.1158/1538-7445.AM2013-LB-120. Abstract nr LB-120 (8 Suppl) (Apr 6-10).

d'Ydewalle, C., Krishnan, J., Chiheb, D.M., Van Damme, P., Irobi, J., Kozikowski, A.P., Vanden Berghe, P., Timmerman, V., Robberecht, W., Van Den Bosch, L., 2011. HDAC6 inhibitors reverse axonal loss in a mouse model of mutant HSPB1-induced Charcot-Marie-Tooth disease. Nat. Med. 17, 968–974. http://dx.doi.org/10.1038/nm.2396nm.2396 [pii].

Yee, A.J., Voorhees, P.M., Bensinger, W., Berdeja, J.G., Supko, J.G., Richardson, P.G., Tamang, D., Jones, S.S., Patrick, G., Wheeler, C., Raje, N., 2014. Ricolinostat (ACY-1215), a selective HDAC6 inhibitor, in combination with lenalidomide and dexamethasone: results of a phase 1b trial in relapsed and relapsed refractory multiple myeloma. Blood 124 (4772 LP-4772).

Yee, A.J., Bensinger, W.I., Supko, J.G., Voorhees, P.M., Berdeja, J.G., Richardson, P.G., Libby, E.N., Wallace, E.E., Birrer, N.E., Burke, J.N., Tamang, D.L., Yang, M., Jones, S.S., Wheeler, C.A., Markelewicz, R.J., Raje, N.S., 2016. Ricolinostat plus lenalidomide, and dexamethasone in relapsed or refractory multiple myeloma: a multicentre phase 1b trial. Lancet Oncol. 17, 1569–1578. http://dx.doi.org/10.1016/S1470-2045(16)30375-8.

Zareba, G., 2009. Phytotherapy for pain relief. Drugs Today (Barc) 45, 445–467. http://dx.doi.org/10.1358/dot.2009.45.6.1354120.

Zhang, Y., Li, N., Caron, C., Matthias, G., Hess, D., Khochbin, S., Matthias, P., 2003. HDAC-6 interacts with and deacetylates tubulin and microtubules in vivo. EMBO J. 22, 1168–1179. http://dx.doi.org/10.1093/emboj/cdg115.

Zhang, Z., Cao, Y., Zhao, W., Guo, L., Liu, W., 2017. HDAC6 serves as a biomarker for the prognosis of patients with renal cell carcinoma. Cancer Biomark. 1–7. http://dx.doi.org/10.3233/CBM-160298.

Züchner, S., Mersiyanova, I.V., Muglia, M., Bissar-Tadmouri, N., Rochelle, J., Dadali, E.L., Zappia, M., Nelis, E., Patitucci, A., Senderek, J., Parman, Y., Evgrafov, O., De Jonghe, P., Takahashi, Y., Tsuji, S., Pericak-Vance, M.A., Quattrone, A., Battologlu, E., Polyakov, A.V., Timmerman, V., Schröder, J.M., Vance, J.M., 2004. Mutations in the mitochondrial GTPase mitofusin 2 cause Charcot-Marie-Tooth neuropathy type 2A. Nat. Genet. 36, 449–451. http://dx.doi.org/10.1038/ng1341.